LETTER

doi:10.1038/nature10900

Decoherence-protected quantum gates for a hybrid solid-state spin register

T. van der Sar[1], Z. H. Wang[2], M. S. Blok[1], H. Bernien[1], T. H. Taminiau[1], D. M. Toyli[3], D. A. Lidar[4], D. D. Awschalom[3], R. Hanson[1] & V. V. Dobrovitski[2]

Protecting the dynamics of coupled quantum systems from decoherence by the environment is a key challenge for solid-state quantum information processing[1,2]. An idle quantum bit (qubit) can be efficiently insulated from the outside world by dynamical decoupling[3], as has recently been demonstrated for individual solid-state qubits[4–9]. However, protecting qubit coherence during a multi-qubit gate is a non-trivial problem[3,10,11]: in general, the decoupling disrupts the interqubit dynamics and hence conflicts with gate operation. This problem is particularly salient for hybrid systems[12–22], in which different types of qubit evolve and decohere at very different rates. Here we present the integration of dynamical decoupling into quantum gates for a standard hybrid system, the electron–nuclear spin register. Our design harnesses the internal resonance in the coupled-spin system to resolve the conflict between gate operation and decoupling. We experimentally demonstrate these gates using a two-qubit register in diamond operating at room temperature. Quantum tomography reveals that the qubits involved in the gate operation are protected as accurately as idle qubits. We also perform Grover's quantum search algorithm[1], and achieve fidelities of more than 90% even though the algorithm run-time exceeds the electron spin dephasing time by two orders of magnitude. Our results directly allow decoherence-protected interface gates between different types of solid-state qubit. Ultimately, quantum gates with integrated decoupling may reach the accuracy threshold for fault-tolerant quantum information processing with solid-state devices[1,11].

Decoherence is a major hurdle in realizing scalable quantum technologies in the solid state. The interqubit dynamics that implement the quantum logic are unavoidably affected by uncontrolled couplings to the solid-state environment, preventing high-fidelity gate performance (Fig. 1a). Dynamical decoupling[3], a technique that uses fast qubit flips to average out the interactions with the environment, is a powerful and practical tool for mitigating decoherence[4–11,23–25]. This approach is particularly promising for the emerging class of hybrid quantum architectures[12–22], in which different types of qubit, such as electron and nuclear spins, superconducting resonators and nanomechanical oscillators, perform different functions. Dynamical decoupling allows each qubit type to be decoupled at its own rate, ensuring uniform coherence protection.

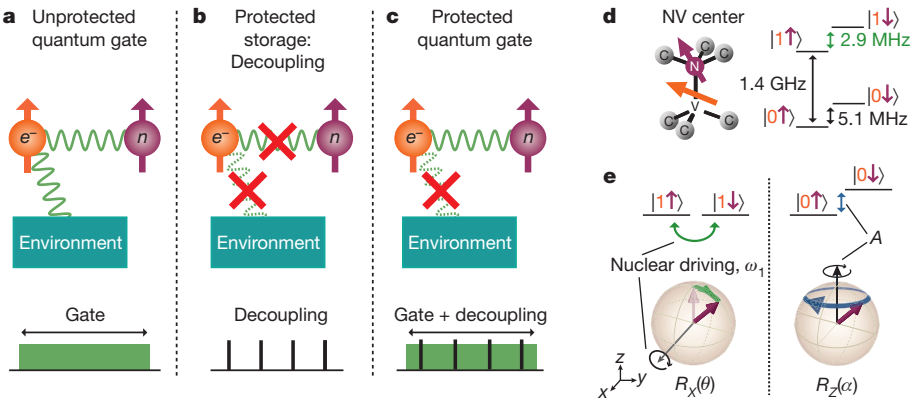

Figure 1 | Quantum gate operation in the presence of decoherence. **a**–**c**, Challenge of high-fidelity quantum gates for qubits (orange, electron spin; purple, nuclear spin) coupled to a decohering environment. **a**, Without decoherence protection, the fidelity of two-qubit gates is limited by interactions with the environment. **b**, Dynamical decoupling efficiently preserves the qubit coherence (protected storage) by turning off the interaction between the qubit and its environment. However, this generally also decouples the qubit from other qubits and prevents two-qubit gate operations. If the decoupling and the gate are separated in time, the unprotected gate is still susceptible to decoherence-induced errors. **c**, The goal is to perform dynamical decoupling during the gate operation, thus ensuring that the gates are protected against decoherence. The gate operation should therefore be compatible with decoupling. The dephasing rate of the nuclear spin is negligible in our experiments. However, nuclear spin protection can easily be incorporated using another layer of decoupling. **d**, The two-qubit system used in this work: a nitrogen–vacancy (NV) colour centre in diamond carries an electron spin $S = 1$ (orange) coupled to a ^{14}N nuclear spin $I = 1$ (purple). The states of the electronic qubit, $|0\rangle$ and $|1\rangle$, are split by 1.4 GHz in an external field $B_0 = 510$ G. The states $|0\uparrow\rangle$ and $|0\downarrow\rangle$ are split by 5.1 MHz owing to nuclear quadrupole and Zeeman interactions. The hyperfine coupling yields an additional splitting, such that the levels $|1\uparrow\rangle$ and $|1\downarrow\rangle$ are separated by 2.9 MHz. The Rabi driving is applied in resonance with this transition. **e**, Dynamics of the electron–nuclear spin system in the limit $\omega_1 \ll A$, visualized in a coordinate frame that rotates with frequency 1.4 GHz in the electron spin subspace and frequency 2.9 MHz in the nuclear spin subspace. In this frame, the states $|1\uparrow\rangle$ and $|1\downarrow\rangle$ have the same energy. The Rabi driving field, which is directed along the x axis, coherently rotates the nuclear spin if the electronic qubit is in $|1\rangle$ (the resulting rotation around the x axis by angle θ is denoted $R_X(\theta)$). However, the Rabi driving is negligible for the states $|0\uparrow\rangle$ and $|0\downarrow\rangle$, which differ in energy by $A = 2\pi \times 2.16$ MHz. The phase accumulation between $|0\uparrow\rangle$ and $|0\downarrow\rangle$ corresponds to a coherent rotation of the nuclear spin around the z axis with frequency A (denoted $R_Z(\alpha)$, where α is the rotation angle).

[1]Kavli Institute of Nanoscience, Delft University of Technology, PO Box 5046, 2600 GA Delft, The Netherlands. [2]Ames Laboratory and Iowa State University, Ames, Iowa 50011, USA. [3]Center for Spintronics and Quantum Computation, University of California, Santa Barbara, California 93106, USA. [4]Departments of Electrical Engineering, Chemistry, and Physics, and Center for Quantum Information Science and Technology, University of Southern California, Los Angeles, California 90089, USA.

However, combining dynamical decoupling with quantum gate operations is generally problematic, because decoupling does not distinguish the desired interqubit interaction from the coupling to the decohering environment, and in general cancels both (Fig. 1b). For hybrid systems, where coherence and control timescales greatly differ among the different qubit types, this problem cannot be remedied by encoding[10] or by the synchronized application of decoupling pulses[3,11] as these require all qubits to be controlled on similar timescales. As a result, decoherence-protected quantum gates in hybrid systems have thus far remained elusive.

Here we present a design that allows the integration of decoupling into gate operation for hybrid quantum architectures. We demonstrate such decoherence-protected gates in a prototype hybrid quantum system: a two-qubit register consisting of an electron and a nuclear spin (Fig. 1c). The key idea is to adapt the time intervals between the electron decoupling pulses precisely to the nuclear spin dynamics. When combined with continuous nuclear spin driving, this yields highly selective rotations of the nuclear spin, and at the same time the electron spin is dynamically protected as explained below. This design preserves all of the advantages of dynamical decoupling without requiring additional qubits or controllable interqubit couplings. It can be readily implemented to yield decoherence-protected quantum gates in a range of hybrid systems, such as various electron–nuclear spin registers[12–16,19], and interface gates between the qubits and a spin-chain quantum data bus[21,22].

We experimentally demonstrate the scheme on a single nitrogen–vacancy centre in diamond[12,15,26–28], where the two qubits are represented by the electron spin and the host ^{14}N nuclear spin (Fig. 1d and Supplementary Information). An entangling gate between these qubits can be implemented using the hyperfine interaction, described by the Hamiltonian $\hat{H}_{\rm hf} = A\hat{I}_Z\hat{S}_Z$, where $A = 2\pi \times 2.16$ MHz for nitrogen–vacancy centres[27,28] and $\hat{I}_Z$ and $\hat{S}_Z$ are respectively the nuclear and electron spin operators. For an unprotected gate, of duration $T_G = \pi/A$, the fidelity is limited by the electron spin dephasing, which is dominated either by the bath of ^{13}C nuclear spins[12] (as in the experiments here) or by the electron spins of substitutional nitrogen atoms[26]. Decoupling applied to the electron spin suppresses decoherence but also disrupts the electron–nucleus coupling. At the same time, synchronized application of the decoupling pulses to both the electronic and the nuclear spin qubit is problematic, because a nuclear spin rotation takes longer (>10 μs in typical experiments[16,27]) than the electron spin's dephasing time, T_2^* (0.5–5 μs for nitrogen–vacancy centres[12,26]; Supplementary Information).

In our gate design, Rabi driving is applied at the frequency of the nuclear spin transition corresponding to the electron spin state $|1\rangle$ ($m_S = -1$; Fig. 1d). In the rotating frame, the two spins are described

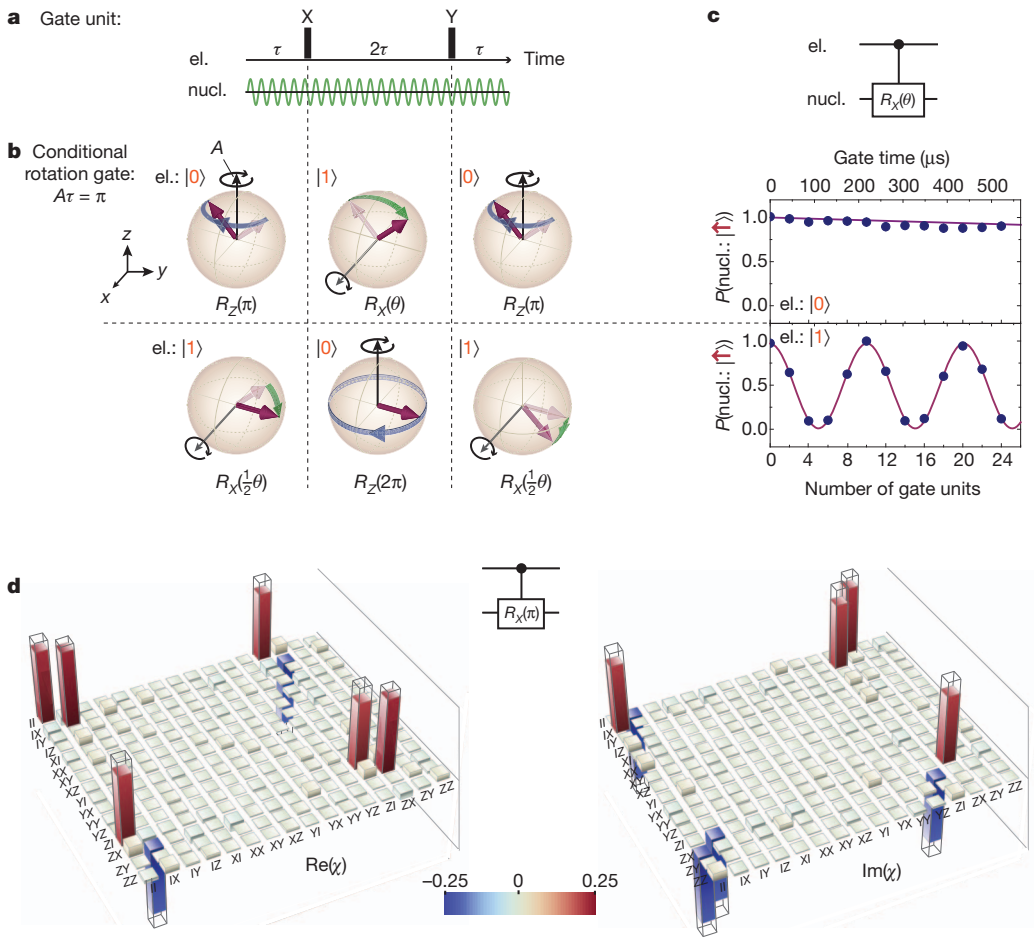

Figure 2 | Decoherence-protected quantum gates for an electron–nuclear spin register. **a**, Basic unit of the decoherence-protected gate, consisting of dynamical decoupling of the electron (el.) spin and continuous nuclear (nucl.) spin driving. X and Y respectively denote electron π-pulses around the *x* and *y* axes, and τ is the delay time. **b**, Bloch spheres showing the nuclear spin dynamics, conditioned on the initial electronic spin state, during a single gate unit. **c**, Decoherence-protected controlled rotation of the nuclear spin. Plotted is the measured probability of the nuclear spin to be in state $|\uparrow\rangle$ as a function of the number of applied gate units, for the two different electron spin input states. Lines are fits taking into account longitudinal relaxation of the electron spin, which was measured independently. For details of the fitting and dynamics of other input states, see Supplementary Information. Error bars corresponding to 1 s.d. are smaller than the data points. **d**, Measured process matrix, χ, of the decoherence-protected CNOT gate. The transparent bars indicate the values of the matrix elements for the ideal gate.

by the Hamiltonian $\hat{H} = A\hat{I}_Z\hat{S}_Z + \omega_1\hat{I}_X$, where ω_1 is the nuclear Rabi frequency. The nuclear spin dynamics is then conditioned on the electron spin state (Fig. 1e and Supplementary Information): the nuclear spin undergoes driven rotation around the x axis if the electron spin is in $|1\rangle$ and precesses around the z axis if the electron is in $|0\rangle$ ($m_S = 0$). Although Fig. 1d shows the case with $\omega_1 \ll A$, which is relevant to our experiments, the scheme works for arbitrary values of ω_1 and A (Supplementary Information).

In parallel with driving the nuclear spin, we decouple the electron spin from the environment using short microwave pulses that constantly switch the electron spin between states $|0\rangle$ and $|1\rangle$ (refs 4, 5, 7). The full decoupling sequence consists of repeating the basic unit τ–X–2τ–Y–τ (Fig. 2a), where X and Y are decoupling pulses that flip the electron spin around the x and y axes, respectively, and 2τ is the interpulse delay. To implement an entangling gate, the nuclear spin dynamics over the full gate unit must depend only on the initial state of the electron spin and cannot be disrupted by the electron's fast switching.

At first, such a condition seems to contradict the very design of the decoupling sequence. However, it may be fulfilled in a special situation where the interpulse delay matches the hyperfine coupling with high precision (at the nanosecond level in our experiments; see Supplementary Information), such that the decoupling pulses are applied in resonance with the rotation of the nuclear spin. This situation provides an opportunity for highly selective coupling of the fast qubit to the targeted slow qubit, while decoupling all others. Experimentally, it is achieved by setting $\tau = (2n + 1)\pi/A$ with integer n, so that the nuclear spin rotates by 180° around the z axis during the interval τ, if the electron is in state $|0\rangle$ during this time. If the electron is in the state $|0\rangle$ during the time interval 2τ, however, the nuclear spin undergoes a 360° rotation that has zero net effect. The overall dynamics during one full gate unit are shown in Fig. 2b: depending on the initial state of the electron, the nuclear spin rotates around the x axis by the angle $\theta = 4\omega_1\tau$ in the clockwise or anticlockwise direction (conditional rotation). An unconditional rotation of the nuclear spin, independent of the electron spin state, is constructed from the same gate unit by choosing $\tau = 2n\pi/A$ (Supplementary Fig. 3). From the conditional and unconditional rotations, we can construct a complete set of gates for the two-qubit register.

We implement the controlled-rotation gate using a conditional nuclear spin rotation followed by an unconditional rotation by the same angle. The experimental data in Fig. 2c confirm the selectivity of this gate: as the number of gate units increases, the nuclear spin rotates around the x axis if the electron spin is initially in state $|1\rangle$, and does nothing if the electron spin is initially in state $|0\rangle$. When the total nuclear rotation angle equals 180°, the gate corresponds to the controlled-NOT (CNOT) gate (neglecting a $\pi/2$ phase shift of the electron spin, which is not relevant here and can be easily corrected). To characterize the CNOT gate fully, we performed quantum process tomography of its action (Fig. 2d). We find an overall process fidelity of $F_p = \mathrm{Tr}(\chi_{ideal}\chi) = 83(1)\%$, where χ is the measured process matrix, χ_{ideal} is the process matrix of the ideal CNOT gate and the parenthetical error is the s.d. This number is a lower bound on the true process fidelity, as it includes errors from imperfect initialization (estimated to be about 5% for this experiment) and errors in the pulses used for state preparation and read-out (estimated to be a few per cent; see Supplementary Information).

A crucial step in this work is testing our design in the presence of stronger decoherence and confirming that it ensures efficient protection during the gate operation. To change the level of decoherence in a

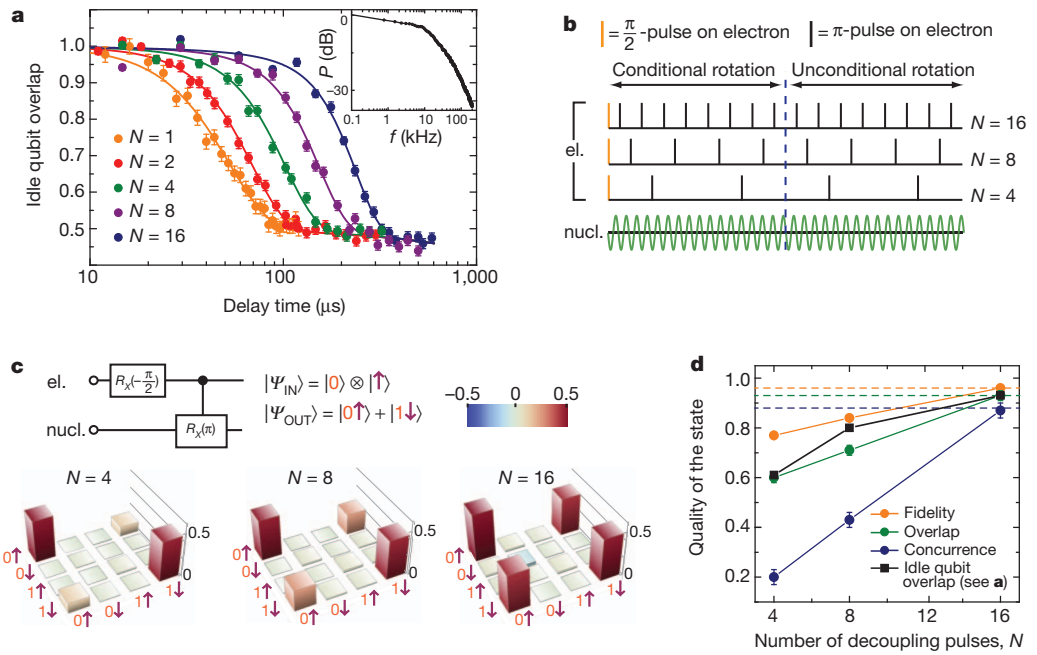

Figure 3 | Performance of the CNOT gate in the presence of strong decoherence. **a**, Dynamical decoupling of the electron spin in the presence of artificially generated low-frequency noise, which is injected into the sample through the same microwave stripline used for the qubit control pulses. The coherence time of the electron spin is effectively prolonged by increasing the number of decoupling pulses, N, in the applied microwave pulse sequence $\pi/2$–$(\tau$–π–$\tau)^N$–$\pi/2$, where τ is the delay time. The points are experimental data and the lines are fits. Fit details are given in Supplementary Information. Inset, power spectrum of the injected noise (P, power; f, frequency; log scale). **b**, Pulse sequences used to test the performance of the CNOT gate for an increasing number of decoupling pulses, N, and a correspondingly decreasing interpulse delay, τ (total gate time is fixed at 120 μs). **c**, Density matrices (real part) of the states created with the pulse sequences shown in **b**. A rotation of the electron spin by $-\pi/2$ about the x axis prepares the state $(|0\rangle + i|1\rangle) \otimes |\uparrow\rangle$, which is transformed into the Bell state $|0\uparrow\rangle + |1\downarrow\rangle$ by a 120-μs CNOT gate. **d**, Fidelity, overlap and concurrence of the states shown in **c**, as functions of the number of decoupling pulses in the CNOT gate. The points are measured data connected by solid lines. The dashed horizontal lines correspond to the performance of the same gate with 16 decoupling pulses in the absence of the artificially generated noise. For comparison, the state overlap for decoupling of an idle electron spin, not involved in gate operation, is also shown (black squares and line). All errors, 1 s.d.

controllable manner, we inject low-frequency noise into the system[23], thus shortening the electron spin-echo decay time, T_2, from 251(7) to 50(2) μs (Fig. 3a). Furthermore, we reduce the nuclear driving power such that the gate time becomes 120 μs, more than twice T_2.

We first verify that the additional decoherence can be efficiently suppressed at the single-qubit level by dynamical decoupling. We observe that the electron spin coherence time increases from 50(2) to 234(8) μs as the number of the decoupling pulses is increased from one (spin echo) to sixteen (Fig. 3a), in agreement with previous studies[4,5,7]. Then we study the fidelity of the CNOT gate as a function of the number of decoupling pulses applied during its 120-μs gate time. The resonance requirements for τ are maintained by decreasing n as the number of pulses is increased (Fig. 3b). We apply the gate to the state $(|0\rangle + i|1\rangle) \otimes |\uparrow\rangle$; this ideally yields the entangled state $|\Psi^+\rangle = |0\uparrow\rangle + |1\downarrow\rangle$ (here $|\uparrow\rangle$ and $|\downarrow\rangle$ correspond to the nuclear spin states with $m_I = +1$ and $m_I = 0$, respectively). Quantum state tomography reveals that the coherence of the output state, corresponding to the off-diagonal elements in the density matrix, ρ, grows rapidly with the number of pulses (Fig. 3c). The state fidelity[1], $F = \sqrt{\langle \Psi^+ | \rho | \Psi^+ \rangle}$, reaches 96(1)% when there are 16 decoupling pulses (Fig. 3d), which corresponds to the overlap $O = \langle \Psi^+ | \rho | \Psi^+ \rangle = 0.92(2)$. Here the gate performs similarly to how it does without the introduced decoherence (Fig. 3d, dashed lines), showing that the gate efficiency remains high even in the regime where the gate time exceeds T_2. Moreover, comparison with single-qubit state fidelities under decoupling (taken from Fig. 3a) demonstrates that the electron spin coherence in the course of the gate operation is preserved as efficiently as it is for an idle electron qubit (Fig. 3d). Numerical simulations provide evidence that the fidelity of the CNOT gate remains high even in the presence of much stronger decoherence caused by nitrogen impurities[4,26] (Supplementary Information), which is highly relevant for scalable quantum architectures in which chains of nitrogen atoms serve as data buses between nitrogen–vacancy centres[21,22].

Finally we illustrate the power of the decoherence-protected gates by implementing a two-qubit algorithm in a hybrid solid-state spin register. We perform Grover's quantum algorithm[1] for searching for a given entry in an unstructured list of L elements. A classical search presents each entry in turn to an 'oracle', which outputs 1 if this is the target entry and outputs 0 otherwise. This requires $\sim L/2$ oracle calls on average. The quantum algorithm encodes each entry as a state of an m-qubit system ($2^m \geq L$) and presents a superposition of all entries to an oracle. The result is processed to increase the weight of the target state in the superposition. After of order $\sqrt{L}$ iterations, this weight becomes close to 1. For two qubits ($L = 4$), a single oracle call is enough to provide an exact answer.

Figure 4a shows all the pulses that implement the algorithm. Because the total execution time, 322 μs, is almost 100 times longer than the electron spin dephasing time, high-fidelity execution of the algorithm is impossible without decoherence protection. The circuit diagram of the full computation is given in Fig. 4b for the target state $|1\downarrow\rangle$, with the conditional phase (CPhase) gate presented separately in Fig. 4c. Figure 4d shows quantum tomographic snapshots of the corresponding two-qubit states at different stages of the algorithm[29]. The fidelity of the resulting state is 95(1)%; for the other target states, the

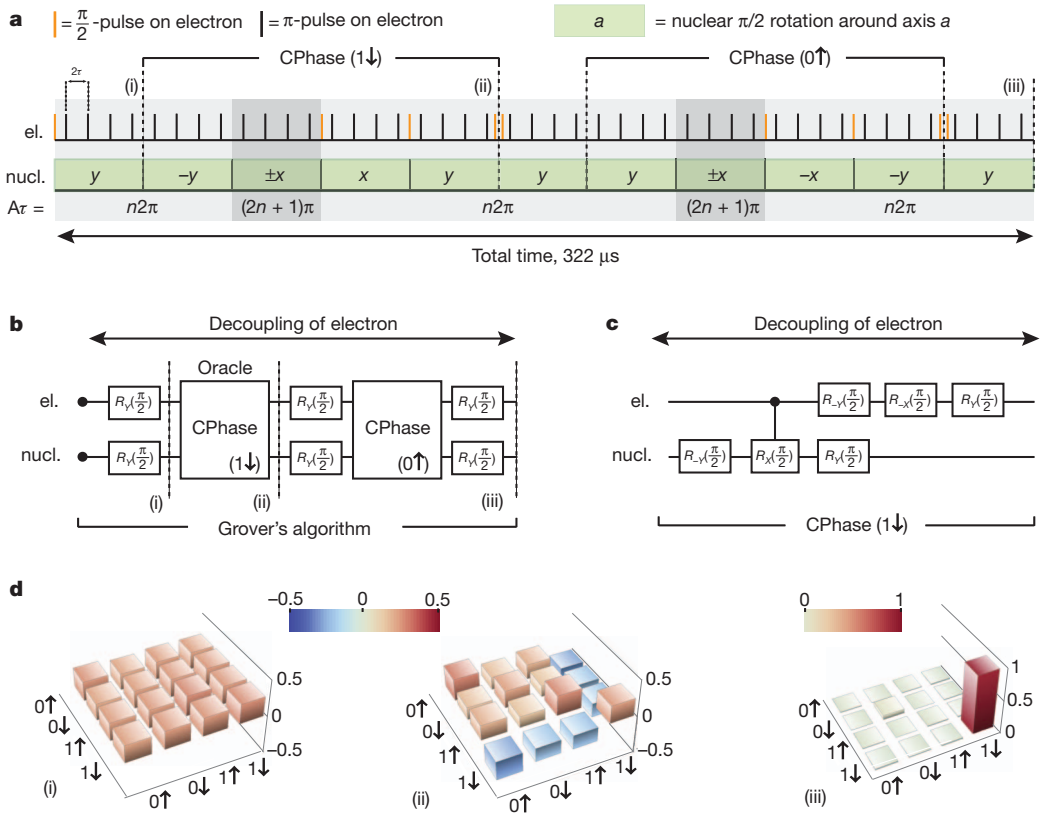

Figure 4 | Grover's search algorithm executed with decoherence-protected gates. **a**, Pulse sequence implementing Grover's algorithm for the target state $|1\downarrow\rangle$. All nuclear spin rotations are implemented with decoherence-protected gates. Each nuclear π/2 rotation is performed using two gate units. The electron and nuclear spin rotation axes are adjusted by changing the phase of the driving field. The total computation time is 322 μs, which exceeds the electron spin-echo decay time, $T_2 = 251$ μs, by about 30%. **b**, Quantum circuit diagram of Grover's algorithm for the target state $|1\downarrow\rangle$, corresponding to the pulse sequence shown in **a**. **c**, Quantum circuit diagram of the CPhase gate, implemented by embedding a CNOT gate between two nuclear π/2-rotation gates that rotate the nuclear spin basis. The pulses on the electron correct the single-qubit phase shift. **d**, Density matrices of the two-qubit system at different stages of Grover's algorithm. Stage (i) corresponds to the initial superposition of all two-qubit states, stage (ii) is the oracle's output and stage (iii) is the final state of the register; see also **a** and **b**. The fidelity of the final state is 95(1)% (overlap, 0.91(3)), mainly limited by longitudinal relaxation of the electron spin.

fidelities are 92(1)% ($|0\uparrow\rangle$), 91(2)% ($|0\downarrow\rangle$) and 91(1)% ($|1\uparrow\rangle$) (Supplementary Information).

Our demonstration of decoherence-protected quantum gates based on resonantly applied decoupling pulses opens the way to high-fidelity transfer, processing and retrieval of quantum information in small quantum registers, which are critical tasks for future quantum repeaters and quantum computers[1,2,13–16,30]. Moreover, our gate design is compatible with quantum error correction and therefore marks an important step towards scalable, fault-tolerant quantum computation in a hybrid qubit architecture.

METHODS SUMMARY

System initialization and read-out. All experiments are performed in a magnetic field of ~510 G aligned parallel to the symmetry axis of the nitrogen–vacancy centre. The two-qubit system is initialized into the $(m_S, m_I) = (0, +1)$ state by 4-μs excitation using a green laser (wavelength, 532 nm; details in Supplementary Information). Electron spin polarization into the $m_S = 0$ state is a result of a spin-dependent relaxation mechanism between the electronic excited state and electronic ground state. At 510 G, a level anticrossing in the electronic excited state allows electron–nuclear spin flip-flops, which, in combination with the mechanism responsible for electron spin polarization, leads to nuclear spin polarization into the $m_I = +1$ state. The state of the system is read out by counting the spin-dependent number of photons emitted into the phonon sideband on green-laser excitation during a detection time window of 1–2 μs (refs 27, 28; details in Supplementary Information).

Influence of longitudinal relaxation of the electron spin. All state fidelity numbers include errors due to spin relaxation within and out of the two-qubit subspace. From independently measured relaxation rates, we estimate that the probabilities to undergo relaxation out of and within the two-qubit subspace are respectively: 0.5% and 0.4% for Fig. 2d, 1% and 0.8% for Fig. 3, and 2.9% and 2.1% for Fig. 4 (Supplementary Information).

Received 6 October 2011; accepted 25 January 2012.

1. Nielsen, M. A. & Chuang, I. L. *Quantum Computation and Quantum Information* (Cambridge Univ. Press, 2000).
2. Ladd, T. D. *et al.* Quantum computers. *Nature* **464,** 45–53 (2010).
3. Viola, L., Lloyd, S. & Knill, E. Universal control of decoupled quantum systems. *Phys. Rev. Lett.* **83,** 4888–4891 (1999).
4. de Lange, G., Wang, Z. H., Ristè, D., Dobrovitski, V. V. & Hanson, R. Universal dynamical decoupling of a single solid-state spin from a spin bath. *Science* **330,** 60–63 (2010).
5. Ryan, C. A., Hodges, J. S. & Cory, D. G. Robust decoupling techniques to extend quantum coherence in diamond. *Phys. Rev. Lett.* **105,** 200402 (2010).
6. Barthel, C., Medford, J., Marcus, C. M., Hanson, M. P. & Gossard, A. C. Interlaced dynamical decoupling and coherent operation of a singlet-triplet qubit. *Phys. Rev. Lett.* **105,** 266808 (2010).
7. Naydenov, B. *et al.* Dynamical decoupling of a single-electron spin at room temperature. *Phys. Rev. B* **83,** 081201 (2011).
8. Bluhm, H. *et al.* Dephasing time of GaAs electron-spin qubits coupled to a nuclear bath exceeding 200 μs. *Nature Phys.* **7,** 109–113 (2011).
9. Bylander, J. *et al.* Noise spectroscopy through dynamical decoupling with a superconducting flux qubit. *Nature Phys.* **7,** 565–570 (2011).
10. West, J. R., Lidar, D. A., Fong, B. H. & Gyure, M. F. High fidelity quantum gates via dynamical decoupling. *Phys. Rev. Lett.* **105,** 230503 (2010).
11. Ng, K.-H., Lidar, D. A. & Preskill, J. Combining dynamical decoupling with fault-tolerant quantum computation. *Phys. Rev. A* **84,** 012305 (2011).
12. Childress, L. *et al.* Coherent dynamics of coupled electron and nuclear spin qubits in diamond. *Science* **314,** 281–285 (2006).
13. Childress, L., Taylor, J. M., Sorensen, A. S. & Lukin, M. D. Fault-tolerant quantum communication based on solid-state photon emitters. *Phys. Rev. Lett.* **96,** 070504 (2006).
14. Morton, J. J. L. *et al.* Solid-state quantum memory using the ^{31}P nuclear spin. *Nature* **455,** 1085–1088 (2008).
15. Neumann, P. *et al.* Multipartite entanglement among single spins in diamond. *Science* **320,** 1326–1329 (2008).
16. Jiang, L. *et al.* Repetitive readout of a single electronic spin via quantum logic with nuclear spin ancillae. *Science* **326,** 267–272 (2009).
17. Kubo, Y. *et al.* Strong coupling of a spin ensemble to a superconducting resonator. *Phys. Rev. Lett.* **105,** 140502 (2010).
18. Rabl, P. *et al.* A quantum spin transducer based on nanoelectromechanical resonator arrays. *Nature Phys.* **6,** 602–608 (2010).
19. Fuchs, G. D., Burkard, G., Klimov, P. & Awschalom, D. D. A quantum memory intrinsic to single nitrogen–vacancy centres in diamond. *Nature Phys.* **7,** 789–793 (2011).
20. Arcizet, O. *et al.* A single nitrogen-vacancy defect coupled to a nanomechanical oscillator. *Nature Phys.* **7,** 879–883 (2011).
21. Cappellaro, P., Viola, L. & Ramanathan, C. Coherent-state transfer via highly mixed quantum spin chain. *Phys. Rev. A* **83,** 032304 (2011).
22. Yao, N. Y. *et al.* Scalable architecture for a room temperature solid-state quantum processor. *Nature Commun.* (in the press); preprint at ⟨http://arxiv.org/abs/1012.2864⟩ (2010).
23. Biercuk, M. J. *et al.* Optimized dynamical decoupling in a model quantum memory. *Nature* **458,** 996–1000 (2009).
24. Sagi, Y., Almog, I. & Davidson, N. Process tomography of dynamical decoupling in a dense cold atomic ensemble. *Phys. Rev. Lett.* **105,** 053201 (2010).
25. Du, J. *et al.* Preserving electron spin coherence in solids by optimal dynamical decoupling. *Nature* **461,** 1265–1268 (2009).
26. Hanson, R., Dobrovitski, V. V., Feiguin, A. E., Gywat, O. & Awschalom, D. D. Coherent dynamics of a single spin interacting with an adjustable spin bath. *Science* **320,** 352–355 (2008).
27. Smeltzer, B., McIntyre, J. & Childress, L. Robust control of individual nuclear spins in diamond. *Phys. Rev. A* **80,** 050302 (2009).
28. Steiner, M., Neumann, P., Beck, J., Jelezko, F. & Wrachtrup, J. Universal enhancement of the optical readout fidelity of single electron spins at nitrogen-vacancy centers in diamond. *Phys. Rev. B* **81,** 035205 (2010).
29. DiCarlo, L. *et al.* Demonstration of two-qubit algorithms with a superconducting quantum processor. *Nature* **460,** 240–244 (2009).
30. Bermudez, A., Jelezko, F., Plenio, M. B. & Retzker, A. Electron-mediated nuclear-spin interactions between distant NV centers. *Phys. Rev. Lett.* **107,** 150503 (2011).

Supplementary Information is linked to the online version of the paper at www.nature.com/nature.

Acknowledgements We thank L. DiCarlo, F. Jelezko, M. D. Lukin and L. M. K. Vandersypen for discussions and comments. T.v.d.S., H.B. and R.H. acknowledge support from the Dutch Organization for Fundamental Research on Matter and the Netherlands Organization for Scientific Research. D.D.A. acknowledges support from DARPA QuEST, AFOSR and ARO MURI, and R.H. acknowledges support from DARPA QuEST. D.A.L. was sponsored by the National Science Foundation under grant numbers CHM-924318, CHM-1037992 and PHY-0969969, ARO MURI grant W911NF-11-1-0268, and by the US Department of Defense. The views and conclusions contained in this document are those of the authors and should not be interpreted as representing the official policies, either expressly or implied, of the US Government. Work at Ames Laboratory was supported by the Department of Energy, Basic Energy Sciences under contract number DE-AC02-07CH11358.

Author Contributions Z.H.W., D.A.L. and V.V.D. designed the gate and did the theoretical analysis. H.B. and D.M.T. made the device. T.v.d.S., M.S.B., T.H.T., D.D.A. and R.H. designed and performed the experiments. T.v.d.S., R.H. and V.V.D. wrote the manuscript. All authors discussed the results and commented on the manuscript.

Author Information Reprints and permissions information is available at www.nature.com/reprints. The authors declare no competing financial interests. Readers are welcome to comment on the online version of this article at www.nature.com/nature. Correspondence and requests for materials should be addressed to V.V.D. (slava@ameslab.gov).